Implementation of the panel method to the solution of flow around aircraft

Yassir ABBAS*,[1], Mohammed MADBOULI[1]

*Corresponding author
*,[1]Aeronautical Engineering Department, Engineering College, Cairo University
Giza State, Egypt
yasirabas75@hotmail.com*, dr_madbouli@hotmil.com

DOI: 10.13111/2066-8201.2015.7.2.1

3rd International Workshop on Numerical Modelling in Aerospace Sciences, NMAS 2015,
06-07 May 2015, Bucharest, Romania, (held at INCAS, B-dul Iuliu Maniu 220, sector 6)
Section 2 – Flight dynamics simulation

Abstract*: In this study a panel method is used as a numerical technique for the solution of the potential three dimensional flows about a complete aircraft configuration to determine the aerodynamic characteristics. This approach seems to be more economic, from the computational point of view than methods that solve the flow field in the whole fluid volume such as finite difference, finite element or finite volume techniques. A system of source and doublet distributions is implemented and Dirichlet boundary conditions are applied. A computer program using Matlab is developed. Firstly flow over three dimensional swept wings is solved and the results are compared with experimental data to validate the numerical panel code. After the ideas have been discussed a sample calculations around complete aircraft are presented to illustrate the gain of using panel method technique.*

Key Words: *aerodynamics, panel method, influence matrix, velocity potential.*

1. INTRODUCTION

The main purpose of this paper is to develop a MATLAB code as a computational tool for the solution of potential flow around three dimensional swept wings and complete aircraft to obtain the aerodynamics characteristics by using the panel method.

Panel method is a technique used for solving the potential flow around 2D and 3D geometries, based on simplifying assumptions about the physics and properties of the flow of air over these geometries. The viscosity and compressibility of air in the flow field is neglected, and the curl of the velocity field is assumed to be zero (no vorticity in the flow field) [1]. Under these assumptions, the vector velocity describing the flow field can be represented as the gradient of a scalar velocity potential, and the resulting flow is referred to as potential flow. A statement of conservation of mass in the flow field leads to Laplace's equation as the governing equation for the velocity potential($\nabla^2 \emptyset = 0$) [2].

The governing equation (Laplace's equation) is recast into an integral equation. The integral equation involves quantities such as velocity, only on the surface, whereas the original equation involved the velocity potential all over the flow field. The surface is divided into panels and the integral is approximated by an algebraic expression on each of these panels. A system of linear algebraic equations results for the unknowns at the solid surface, which may be solved to determine the unknowns at the body surface [3].

Panel programs can be subdivided into two groups: low order and high order. In a low order panel method, singularities are distributed with constant strength over each panel, while in a higher order method, singularity strengths are allowed to vary linearly or quadratic over each panel [4].

The first paper on a practical three-dimensional method to solve the linearized potential equations was published by Hess and Smith [5]. Their method itself was simplified, in that it did not include lifting flows and hence was mainly applied to ship hulls and aircraft fuselages. The first lifting Panel Code (A230) was described in a paper written by Paul Rubbert and Gary Saaris of Boeing Aircraft in 1968. In time, more advanced three-dimensional panel codes were developed at Boeing (PANAIR,A502), Lockheed (Quadpan), Douglas (HESS), McDonnell Aircraft (MACAERO), NASA (PMARC) and Analytical Methods (WBAERO, USAERO and VSAERO) [6].

2. PROBLEM FORMULATION

The problem under consideration in this paper is that of the potential flow of an incompressible, inviscid flow. The exact solution of the potential flow for arbitrary boundaries can be approached in a variety of ways, all of which must finally become numerical and make use of a computing machine. More efficient methods are based on the reduction of the problem to integral equations over the boundary surface. Finally the integral equations may be approximated by a set of linear algebraic equations which are solved by any of the usual techniques.

3. INTEGRAL EQUATIONS OF POTENTIAL FLOW

Integral equations of potential flow are formed in suitable forms for use in panel method calculations. Starting with the Gauss Divergence theorem which relates a volume integral and a surface integral, [6]:

$$\int_V \nabla A dV = \int_S A.ndS, \tag{1}$$

Consider the problem as shown in figure (1):

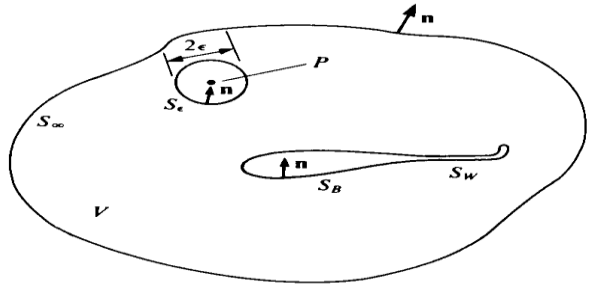

Figure 1: Nomenclature used to define the potential flow problem [7]

Introducing the vector (**A**):

$$\mathbf{A} = \phi_1 \nabla \phi_2 - \phi_2 \nabla \phi_1 \tag{2}$$

where ϕ_1, ϕ_2 are two scalar functions of position. By substitution in equation (1):

$$\int_V \nabla(\phi_1 \nabla\phi_2 - \phi_2 \nabla\phi_1) dV = \int_S (\phi_1 \nabla\phi_2 - \phi_2 \nabla\phi_1).ndS, \tag{3}$$

Once $\nabla(\phi_1 \nabla\phi_2 - \phi_2 \nabla\phi_1)$ is equal to $(\phi_1 \nabla^2\phi_2 - \phi_2 \nabla^2\phi_1)$, then:

$$\int_V (\phi_1 \nabla^2\phi_2 - \phi_2 \nabla^2\phi_1) dV = \int_S (\phi_1 \nabla\phi_2 - \phi_2 \nabla\phi_1).ndS \tag{4}$$

where: $S = S_B + S_W + S_\infty + S_\varepsilon$

By defining $\phi_1 = \frac{1}{r}$ and $\phi_2 = \phi$, where ϕ is the potential (a function that satisfies Laplace's equation) of the flow of interest in V, and r is the distance from the interest point $P(x, y, z)$ as shown in figure (1). The $\frac{1}{r}$ term is a source singularity in three dimensions. Then equation (4) can be rewrite using these terms as:

$$\int_V \left(\frac{1}{r}\nabla^2\phi - \phi\nabla^2\left(\frac{1}{r}\right)\right) dV = \int_S \left(\frac{1}{r}\nabla\phi - \phi\nabla\left(\frac{1}{r}\right)\right).ndS \tag{5}$$

The region V is enclosed by the surface S_∞. Recognize that on the left hand side of equation (5) the first term ($\nabla^2\phi$) is equal to zero, so equation (5) becomes:

$$-\int_V \phi\nabla^2\left(\frac{1}{r}\right) dV = \int_S \left(\frac{1}{r}\nabla\phi - \phi\nabla\left(\frac{1}{r}\right)\right).ndS \tag{6}$$

If point P is external to the S, then $\nabla^2\left(\frac{1}{r}\right) = 0$ everywhere since $\frac{1}{r}$ is the source, and thus satisfies Laplace's equation. This leaves the left hand side of equation (6) equal to zero, with the following result: [8]

$$\int_S \left(\frac{1}{r}\nabla\phi - \phi\nabla\left(\frac{1}{r}\right)\right).ndS = 0 \tag{7}$$

If point P is inside the S, then $\nabla^2\left(\frac{1}{r}\right) \to \infty$ at $r = 0$, therefore we exclude this point by defining a new region which excludes the origin by drawing a sphere of radius ε around $r = 0$, and applying equation (7) to the region between ε and S :[8]

$$\underbrace{\int_S \left(\frac{1}{r}\nabla\phi - \phi\nabla\left(\frac{1}{r}\right)\right).ndS}_{arbitrary\quad region} = \underbrace{\int_\varepsilon \left(\frac{1}{r}\frac{\partial\phi}{\partial r} + \frac{\phi}{r^2}\right) dS}_{sphere} \tag{8}$$

Consider the first integral on the left hand side of equation (8), let $\varepsilon \to 0$, where $(as \quad \varepsilon \to 0)$, we take $\phi \approx$ constant $\left(\frac{\partial\phi}{\partial r} = 0\right)$, assuming that ϕ is well-behaved and using

the mean value theorem. Then evaluate $\iint_{\varepsilon} \frac{dS}{r^2}$ over the surface of the sphere where $\varepsilon = r$. For sphere the elemental area as seen from figure (2) is:

$$dS = r^2 \sin\theta \, d\theta \, d\phi \tag{9}$$

By substituting into the integral:

$$\iint_{\varepsilon} \frac{dS}{r^2} = \iint_{\varepsilon} \frac{r^2 \sin\theta \, d\theta \, d\phi}{r^2} = \iint_{\varepsilon} \sin\theta \, d\theta \, d\phi \tag{10}$$

Integration from $\theta = 0$ *to* π and $\phi = 0$ *to* 2π, we get:

$$\int_{\phi=0}^{\phi=2\pi} \int_{\theta=0}^{\theta=\pi} \sin\theta \, d\theta \, d\phi = 4\pi \tag{11}$$

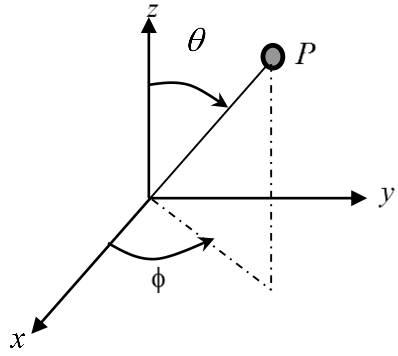

Figure 2: Nomenclature of spherical coordinate system [6]

The final result for the right side integral in equation (8) is:

$$\iint_{\varepsilon} \left(\frac{1}{r} \frac{\partial\phi}{\partial r} + \frac{\phi}{r^2} \right) dS = 4\pi\phi \tag{12}$$

Replacing this integral by its value into equation (8), the expression for the potential at any point P as (where the origin can be placed anywhere inside the region S):

$$\phi(P) = \frac{1}{4\pi} \int_{S} \left(\frac{1}{r} \nabla\phi - \phi \nabla\left(\frac{1}{r} \right) \right) . n dS \tag{13}$$

And the value of ϕ at any point P in the flow, within the region V is now known as a function of ϕ and $\frac{\partial\phi}{\partial n}$ on the boundaries S. In equation (13) S is $S_B + S_W + S_\infty$. If the flow of interest occurs inside the boundary of S_B, and the resulting "internal potential" is ϕ_i, for this flow the point P (which in the region V) is exterior to S_B, then:

$$\frac{1}{4\pi} \int_{S_B} \left(\frac{1}{r} \nabla\phi_i - \phi_i \nabla\left(\frac{1}{r} \right) \right) . n dS = 0 \tag{14}$$

Equation (13) becomes:

$$\phi(P)=\frac{1}{4\pi}\int_{S_B}\left(\frac{1}{r}\nabla(\phi-\phi_i)-(\phi-\phi_i)\nabla\left(\frac{1}{r}\right)\right).ndS+\frac{1}{4\pi}\int_{S_W+S_\infty}\left(\frac{1}{r}\nabla\phi-\phi\nabla\frac{1}{r}\right).ndS \tag{15}$$

The $(\frac{1}{r})$ in the above equation (15) can be interpreted as a source of strength $\frac{\partial\phi}{\partial n}$, and the $\nabla\left(\frac{1}{r}\right)$ term as a doublet of strength ϕ. Therefore, we can find the potential as a function of a distribution of sources and doublets on the surface. In equation (15), $(\phi-\phi_i)$ is the difference between the external and internal potentials.

When S_∞ is considered to be far from S_B the potential can be defined as $\phi_\infty(P)$:

$$\phi_\infty(P)=\frac{1}{4\pi}\int_{S_\infty}\left(\frac{1}{r}\nabla\phi-\phi\nabla\frac{1}{r}\right).ndS \tag{16}$$

Equation (15) becomes:

$$\phi(P)=\frac{1}{4\pi}\int_{S_B}\left(\frac{1}{r}\nabla(\phi-\phi_i)-(\phi-\phi_i)\nabla\left(\frac{1}{r}\right)\right).ndS+\frac{1}{4\pi}\int_{S_W}\left(\frac{1}{r}\nabla\phi-\phi\nabla\frac{1}{r}\right).ndS+\phi_\infty(P) \tag{17}$$

The wake is generally considered to be infinitely thin (not solid surface); with $\frac{\partial\phi}{\partial n}=0$ therefore only doublets are used to represent the wakes. Then equation (17) becomes:

$$\phi(P)=\frac{1}{4\pi}\int_{S_B}\left(\frac{1}{r}\nabla(\phi-\phi_i)-(\phi-\phi_i)\nabla\left(\frac{1}{r}\right)\right).ndS-\frac{1}{4\pi}\int_{S_W}\phi\, n.\nabla\frac{1}{r}dS+\phi_\infty(P) \tag{18}$$

This formula, equation (18), gives the value of $\phi(P)$ at any point in the flow within the region V as a function of ϕ and $\frac{\partial\phi}{\partial n}$ (denote the differentiating in the direction of the outwards normal to the surface S_B) on the boundary.

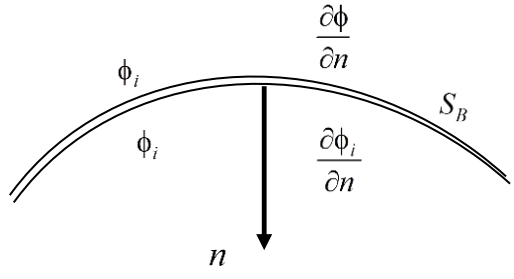

Figure 3: The velocity potential near solid boundary [7]

To define the difference between the external and internal potentials $(\phi-\phi_i)$, consider the segment of the boundary S_B as shown in figure (3), is:

$$-\mu=\phi-\phi_i \tag{19}$$

The difference between the normal derivatives of the external and internal potentials is defined as:

$$-\sigma = \frac{\partial \phi}{\partial n} - \frac{\partial \phi_i}{\partial n} \tag{20}$$

On the boundaries $\phi_i = 0$ and $\frac{\partial \phi_i}{\partial n} = 0$. The source strength is required to be:

$$\sigma = n.\phi_\infty \tag{21}$$

These elements are called doublet (μ) and source (σ), and the minus sign is a result of the normal vector n pointing into S_B. The vector n here is the local normal to the surface, which points in the doublet direction; there it is convenient to replace $n.\nabla$ by $\frac{\partial \phi}{\partial n}$. By these terms equation (18) becomes:

$$\phi(P) = -\frac{1}{4\pi}\int_{S_B}\left(\sigma\left(\frac{1}{r}\right) - \mu\frac{\partial}{\partial n}\left(\frac{1}{r}\right)\right)dS + \frac{1}{4\pi}\int_{S_W}\left(\mu\frac{\partial}{\partial n}\left(\frac{1}{r}\right)\right)dS + \phi_\infty(P) \tag{22}$$

The problem is to find the values of the unknown source σ and doublet μ strengths for a specific geometry and given free stream ϕ_∞. In addition, equation (22) now has an integral equation to solve for the unknown surface singularity distributions instead of a partial differential equation. The problem is linear, allowing us to use superposition to construct solutions.

4. REDUCTION OF THE PROBLEM TO A SET OF LINEAR ALGEBRAIC EQUATIONS

Equation (22) is the basis of many numerical solutions of potential flow, to describes and solves the flow it is important to set the problem in form of algebraic equations. The approach adopted consists of approximating equation (22) by a set of linear algebraic equations. The boundary or body surface about which the flow is to be computed is approximated by a large number of surface elements, whose characteristics dimensions are small compared to those of the body.

Consider a body with known boundaries S_B submerged in a potential flow as shown in figure (4). The flow of interest is in the outer region V where incompressible, irrotational continuity equation, in the body's frame of reference, in terms of the total potential ϕ^* is:

$$\nabla^2\phi^* = 0 \tag{23}$$

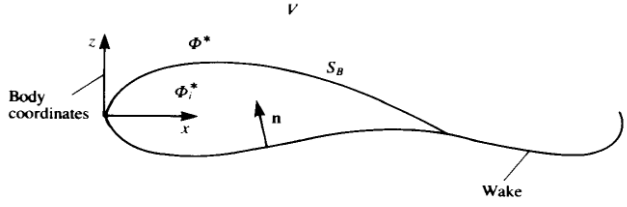

Figure 4: Potential flow over a closed body [7]

The solution of equation (23) is constructed by a sum of source σ and doublet μ distributions placed on the boundaries S_B as:

$$\phi^*(x, y, z) = -\frac{1}{4\pi}\int_{S_B}\left(\sigma\left(\frac{1}{r}\right) - \mu\frac{\partial}{\partial n}\left(\frac{1}{r}\right)\right)dS + \phi_\infty \tag{24}$$

Where ϕ_∞ is the free stream potential ($U_\infty x + V_\infty y + W_\infty z$). If the wake is modeled by a thin doublet sheet, equation (24) can be written as:

$$\phi^*(x, y, z) = \frac{1}{4\pi}\int_{body+wake}\mu\frac{\partial}{\partial n}\left(\frac{1}{r}\right)dS - \frac{1}{4\pi}\int_{body}\sigma\left(\frac{1}{r}\right)dS + \phi_\infty \tag{25}$$

When applying the Dirichlet boundary condition by specifying ϕ^* on the boundaries S_B, and distributing the singularity elements on the surface (the point (x, y, z) inside the surface S_B) the inner potential ϕ_i^* in terms of singularity distribution is obtained as:

$$\phi_i^*(x, y, z) = \frac{1}{4\pi}\int_{body+wake}\mu\frac{\partial}{\partial n}\left(\frac{1}{r}\right)dS - \frac{1}{4\pi}\int_{body}\sigma\left(\frac{1}{r}\right)dS + \phi_\infty \tag{26}$$

On the solid boundaries S_B the condition:

$$\nabla(\phi + \phi_\infty).n = 0 \tag{27}$$

In terms of velocity potential, becomes:

$$\phi_i^* = (\phi + \phi_\infty)_i = cons. \tag{28}$$

Equation (26) becomes:

$$\phi_i^*(x, y, z) = \frac{1}{4\pi}\int_{body+wake}\mu\frac{\partial}{\partial n}\left(\frac{1}{r}\right)dS - \frac{1}{4\pi}\int_{body}\sigma\left(\frac{1}{r}\right)dS + \phi_\infty = cons. \tag{29}$$

The solution to equation (29) depends on the value of the inner potential ϕ_i^*, when the inner potential is set to be $\phi_i^* = (\phi + \phi_\infty)_i = \phi$, the equation reduced to:

$$\frac{1}{4\pi}\int_{body+wake}\mu\frac{\partial}{\partial n}\left(\frac{1}{r}\right)dS - \frac{1}{4\pi}\int_{body}\sigma\left(\frac{1}{r}\right)dS = 0 \tag{30}$$

In order to solve equation (30) numerically, the surface boundary S_B and the wake S_W are divided to N_B surface panels and N_W wake panels as shown in figure (5) and the boundary conditions are specified at the collocation points.

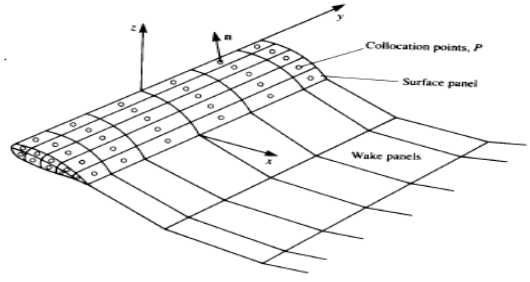

Figure 5: Discretization of the wing surface and wake [7]

By using Dirichlet boundary condition for each of the collocation points, equation (30) can be written as:

$$\sum_{i=1}^{N_B}\frac{1}{4\pi}\int_{body}\mu\frac{\partial}{\partial n}\left(\frac{1}{r}\right)dS+\sum_{j=1}^{N_W}\frac{1}{4\pi}\int_{wake}\mu\frac{\partial}{\partial n}\left(\frac{1}{r}\right)dS-\sum_{i=1}^{N_B}\frac{1}{4\pi}\int_{body}\sigma\left(\frac{1}{r}\right)dS=0 \tag{31}$$

The first and third integrals of the above equation are carried out over each panel of the body surface S_B and the second integral is taken over each panel of the wake panel S_W, thus the summation of the influences of all i body panels and j wake panels is needed in order to confirm that the boundary condition is satisfied. For the panel geometry the quadrilateral panel is used to represent the body and wake panels as shown in figure (6):

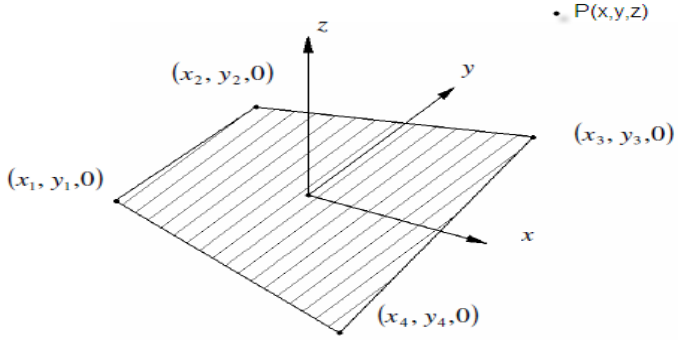

Figure 6: Geometry of the panel [7]

The quadrilateral panel defined by four corners $(1,2,3,4)$, for constant strength element equation (31) can be written as:

$$\sum_{i=1}^{N_B}\frac{\mu}{4\pi}\int_{body}\frac{\partial}{\partial n}\left(\frac{1}{r}\right)dS+\sum_{j=1}^{N_W}\frac{\mu}{4\pi}\int_{wake}\frac{\partial}{\partial n}\left(\frac{1}{r}\right)dS-\sum_{i=1}^{N_B}\frac{\sigma}{4\pi}\int_{body}\left(\frac{1}{r}\right)dS=0 \tag{32}$$

For a constant strength μ element: $\frac{1}{4\pi}\int_{body}\frac{\partial}{\partial n}\left(\frac{1}{r}\right)dS\equiv C_i$, $\frac{1}{4\pi}\int_{wake}\frac{\partial}{\partial n}\left(\frac{1}{r}\right)dS\equiv C_j$. For a constant strength σ element: $-\frac{1}{4\pi}\int_{body}\left(\frac{1}{r}\right)dS\equiv B_i$, C_i, C_j, B_i are the influence coefficients (defined as the velocities induced at a control points) of the panel. These integrals are a function of points 1,2,3,4 and P only.

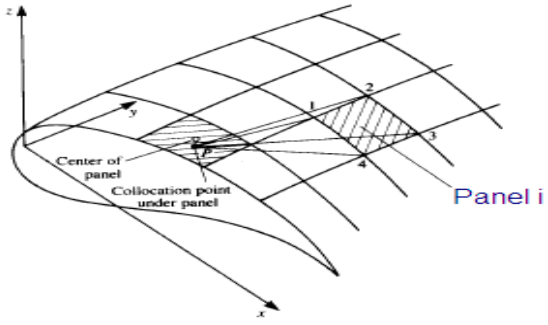

Figure 7: Influence of panel i on point P [7]

After computing the influence of each panel on each other panel equation (31) for each point P inside the body in terms of influence coefficients becomes:

$$\sum_{i=1}^{N_B} C_i \mu_i + \sum_{j=1}^{N_W} C_j \mu_j + \sum_{i=1}^{N_B} B_i \sigma_i = 0 \tag{33}$$

Equation (33) can be evaluated for each collocation point inside the body.

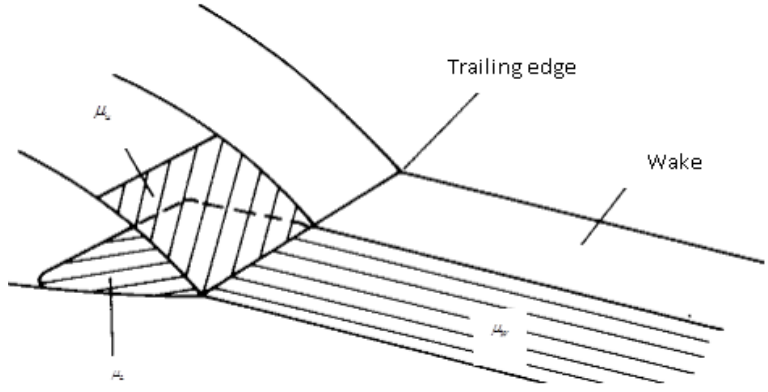

Figure 8: Relation between trailing edge upper and lower panel doublet strength and wake doublet strength [7]

From figure (8) it is clear that there is a relation between the trailing edge upper and lower doublet strength and the wake doublet strength as:

$$\mu_w = \mu_u - \mu_l \tag{34}$$

The influence of wake element becomes:

$$\sum_{j=1}^{N_W} C_j \mu_j = \sum_{j=1}^{N_W} C_j \left(\mu_u - \mu_l\right)_j \tag{35}$$

This algebraic relation can be substituted into the C_i coefficients of the unknown surface doublets such that:

$A_i = C_i$ if panel is not at trailing edge.

$A_i = C_i + C_j$ if panel at upper surface of the trailing edge.

$A_i = C_i - C_j$ if panel at lower surface of the trailing edge.

Equation (33) becomes:

$$\sum_{i=1}^{N} A_i \mu_i + \sum_{i=1}^{N} B_i \sigma_i = 0 \tag{36}$$

Where *A* and *B* are influence coefficients.

The source strength σ is known from equation (21), thus equation (36) becomes:

$$\sum_{i=1}^{N} A_i \mu_i = -\sum_{i=1}^{N} B_i \sigma_i \tag{37}$$

Calculation of equation (37) at each N control point ($i = 1 \rightarrow N$) results in the following equation with unknown μ_i:

$$\begin{bmatrix} a_{11} & a_{12} & - & - & - & a_{1N} \\ a_{21} & a_{22} & - & - & - & a_{2N} \\ - & - & - & - & - & - \\ - & - & - & - & - & - \\ a_{N1} & a_{N2} & - & - & - & a_{NN} \end{bmatrix} \begin{bmatrix} \mu_1 \\ \mu_2 \\ - \\ - \\ \mu_N \end{bmatrix} = - \begin{bmatrix} b_{11} & b_{12} & - & - & - & b_{1N} \\ b_{21} & b_{22} & - & - & - & b_{2N} \\ - & - & - & - & - & - \\ - & - & - & - & - & - \\ b_{N1} & b_{N2} & - & - & - & b_{NN} \end{bmatrix} \begin{bmatrix} \sigma_1 \\ \sigma_2 \\ - \\ - \\ \sigma_N \end{bmatrix} \tag{38}$$

The right hand side of equation (38) is known, thus:

$$\begin{bmatrix} a_{11} & a_{12} & - & - & - & a_{1N} \\ a_{21} & a_{22} & - & - & - & a_{2N} \\ - & - & - & - & - & - \\ - & - & - & - & - & - \\ a_{N1} & a_{N2} & - & - & - & a_{NN} \end{bmatrix} \begin{bmatrix} \mu_1 \\ \mu_2 \\ - \\ - \\ \mu_N \end{bmatrix} = \begin{bmatrix} RHS_1 \\ RHS_2 \\ - \\ - \\ RHS_N \end{bmatrix} \tag{39}$$

The values of μ_i can be computed by solving this full matrix equation.

5. CALCULATION OF PRESSURE DISTRIBUTIONS AND AERODYNAMIC LOADS

After the solution of equation (39) for the unknowns μ_i the velocity components are evaluated in terms of panel local coordinates (l, m, n) as shown in figure (9) below:

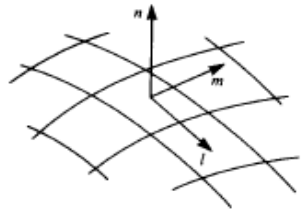

Figure 9: Panel local coordinate system for evaluating the tangential velocity components [7]

$$q_l = \frac{\partial \mu}{\partial l},\ q_m = \frac{\partial \mu}{\partial m},\ q_n = -\sigma_i \tag{40}$$

The total velocity in the local (l, m, n) direction of the panel i is:

$$q_i = \left(q_{\infty_l}, q_{\infty_m}, q_{\infty_n}\right)_i + \left(q_l, q_m, q_n\right)_i \tag{41}$$

From the above equation the value of the velocity component at each control point is:

$$u_i = u_{\infty_l} + \frac{\partial \mu_i}{\partial l} \tag{42}$$

$$v_i = v_{\infty_m} + \frac{\partial \mu_i}{\partial m} \tag{43}$$

$$w_i = w_{\infty_l} - \sigma_i \tag{44}$$

The pressure coefficient is calculated as:

$$C_{P_i} = 1 - \left(\frac{V_i}{V_\infty}\right)^2 \tag{45}$$

where: $V_i = \sqrt{u_i^2 + v_i^2 + w_i^2}$

The contribution of each panel to the non-dimensional fluid dynamic loads is normal to the panel surface and is:

$$\Delta C_{F_i} = \frac{\Delta F_i}{\frac{1}{2}\rho V_i^2 S} \tag{46}$$

In terms of the pressure coefficient the panel contribution to the fluid dynamics load becomes:

$$\Delta C_{F_i} = -\frac{C_{P_i}\Delta S_i}{S}.n_i \tag{47}$$

The individual contributions of the panel elements now can be summed up to compute the desired aerodynamic forces and moments. The forces can be obtained as:

$$F_k = -\sum_{i=1}^{N} C_{p_i} S_i n_{ki} q \qquad , k = x, y, z \tag{48}$$

The moments also obtained as:

$$L = \sum_{i=1}^{N} C_{p_i} S_i n_{yi} q c_{zi} - \sum_{i=1}^{N} C_{p_i} S_i n_{zi} q c_{yi} \tag{49}$$

$$M = -\sum_{i=1}^{N} C_{p_i} S_i n_{xi} q c_{zi} + \sum_{i=1}^{N} C_{p_i} S_i n_{zi} q c_{xi} \tag{50}$$

$$N = \sum_{i=1}^{N} C_{p_i} S_i n_{xi} q c_{yi} - \sum_{i=1}^{N} C_{p_i} S_i n_{yi} q c_{xi} \tag{51}$$

6. ANALYSIS

6.1 Flow around a finite swept wings

The actual wing is replaced by a number of panels with distributions of singularities. The grid cover the wing subdivides it into a number of small panels. On each panel the particular singularity strength is held constant. Flow around swept wings with NACA0015, NACA2412 and NACA64A010 airfoil sections is investigated. The results for the C_P distributions at upper and lower surfaces of the wing with NACA0015 airfoil section at $\alpha = 4^0$ are shown in figure (10) and the difference in pressure distribution is clear between the lower surface and the upper surface.

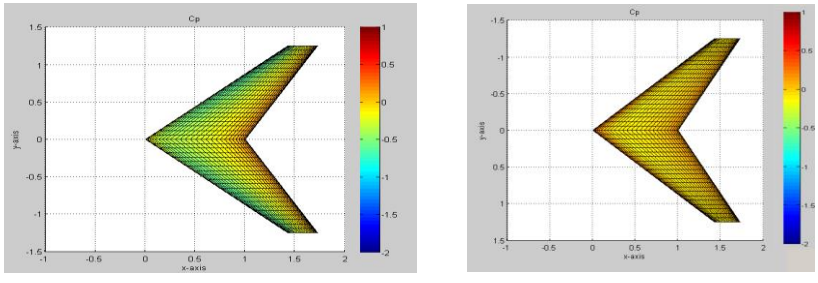

Figure 10: Pressure distributions at upper surface (left) and lower surface (right)

The below figures (11,12 and 13) show the validation for the panel code with experimental published data for the wings with NACA0015, NACA64A010 and NACA2412 airfoil sections, a good agreement is shown.

The difference between the values at higher angles of attack is due to the neglecting of the viscosity in potential flow calculations.

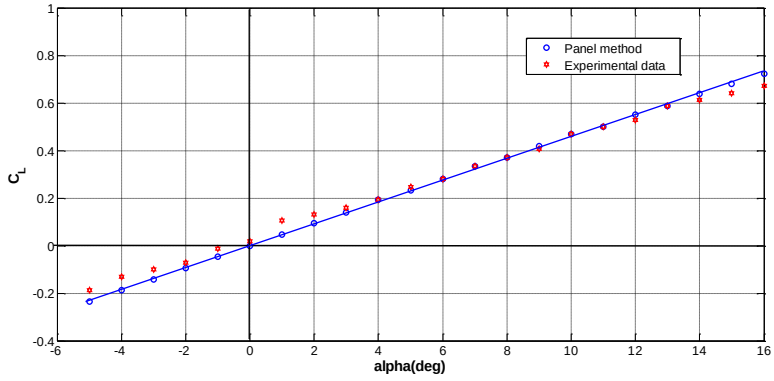

Figure 11: Comparison between lift coefficients for swept back symmetrical wing with NACA0015 airfoil section

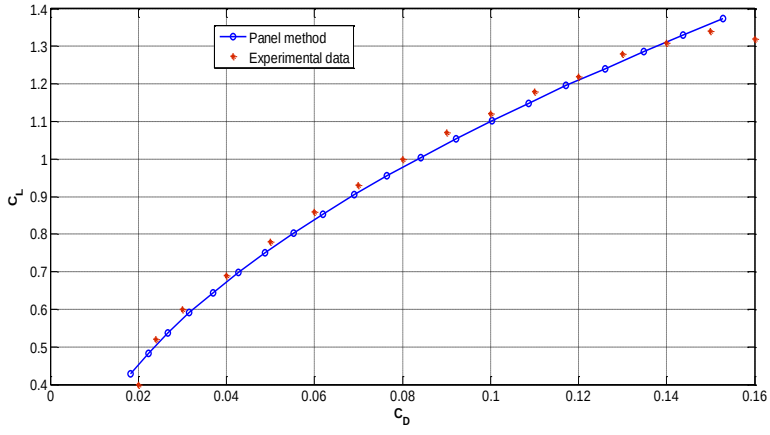

Figure 12: Comparison between drag polar for swept back cambered wing with NACA2412 airfoil section

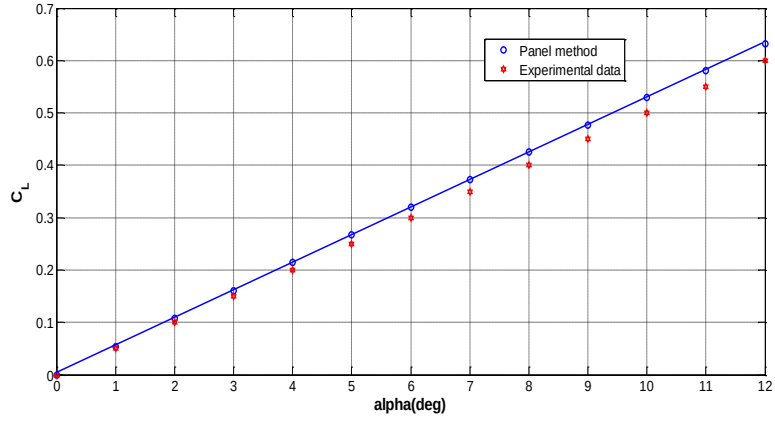

Figure 13: Comparison between lift coefficients for swept back wing with NACA64A010 airfoil section

6.2 Flow around a complete aircraft

Figure 14 shows the grid for Airbus A380 aircraft used, from where the numerical solution was obtained. A comparison was made between the DATCOM and numerical results from the panel method code as in figures 15 and 16.

The more important effect of the elevator in pitching moment is to provide the stability for the aircraft, to keep it flying straight. Figure 17 shows the contributions of elevator to the lift coefficient. Figures 18 and 19 indicate the contributions of the rudder to the rolling and yawing moment.

The rudder usually when deflected, it provides a strong yawing moment and some rolling moments.

Figures 20 and 21 illustrate the effect of the aileron deflection on rolling and yawing moment coefficients, when the aircraft is banked the natural tendency of the aircraft is to slip in the direction of the turn because the lower wing is producing less lift, so the airflow will strikes the side of the aircraft and large surface as the fin which are behind the center of gravity therefore causing the nose to yaw in the direction of the turn. At roll the lift increases on the wing with the downward-deflected aileron because the deflection effectively increases the camber of that portion of the wing.

Conversely, lift decreases on the wing with the upward-deflected aileron since the camber is decreased.

The result of this difference in lift is that wing with more lift rolls upward to create the desired rolling motion.

Unfortunately, drag is also affected by this aileron deflection. More specifically, the drag, is increased when ailerons are deployed.

Thus, the wing on which the aileron is deflected downward to generate more lift also experiences more drag than the other wing.

However, the drag on each side is not equal, and a larger total drag force exists on the wing with the down aileron.

This difference in drag creates a yawing motion in the opposite direction of the roll. Since the yaw motion partially counteracts the desired roll motion, this is known as adverse yaw. Thus the deflection of the ailerons leads to additional yawing moments once the aircraft starts to roll.

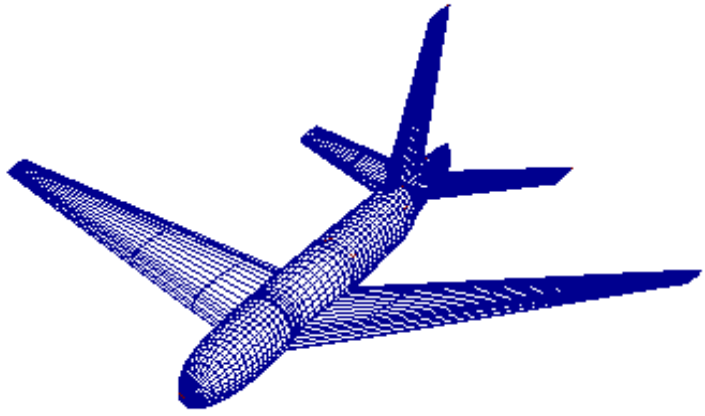

Figure 14: Airbus A380

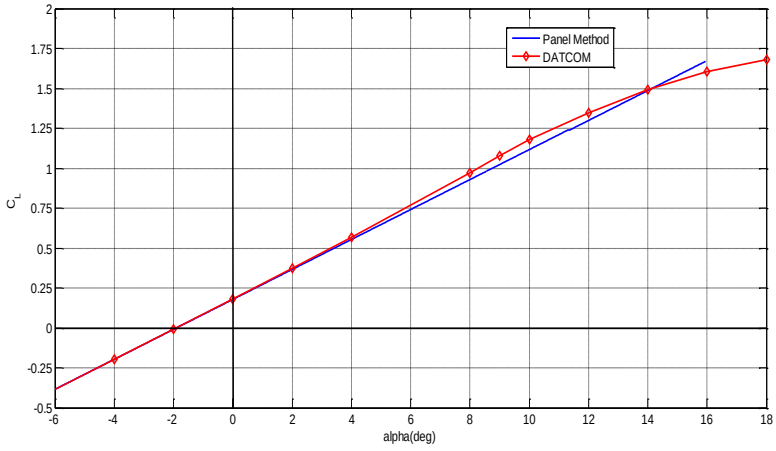

Figure 15: Comparison of lift coefficient obtained from panel code with DATCOM

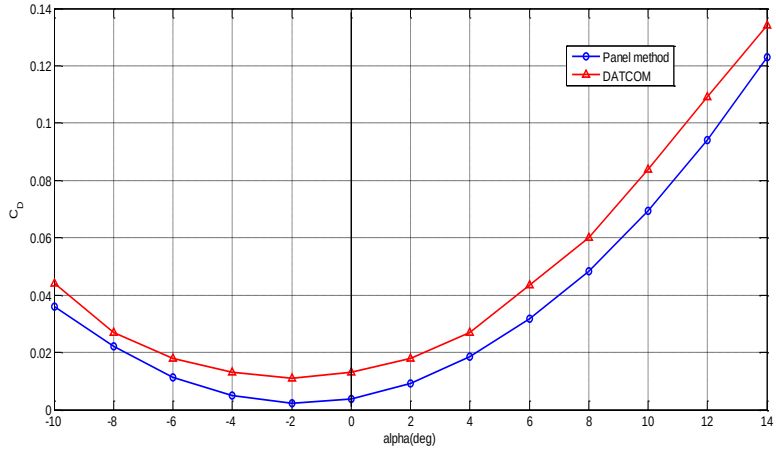

Figure 16: Comparison of drag coefficient obtained from panel code with DATCOM

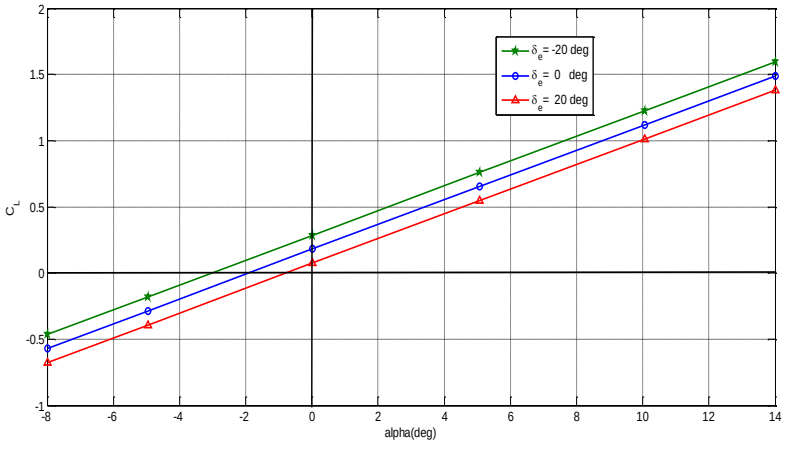

Figure 17: Variation of lift coefficient curve with elevator deflection

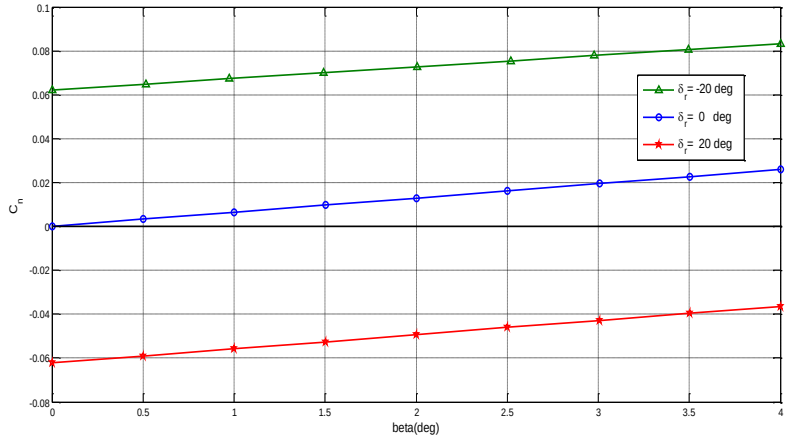

Figure 18: Variation of yawing moment coefficient curve with rudder deflection

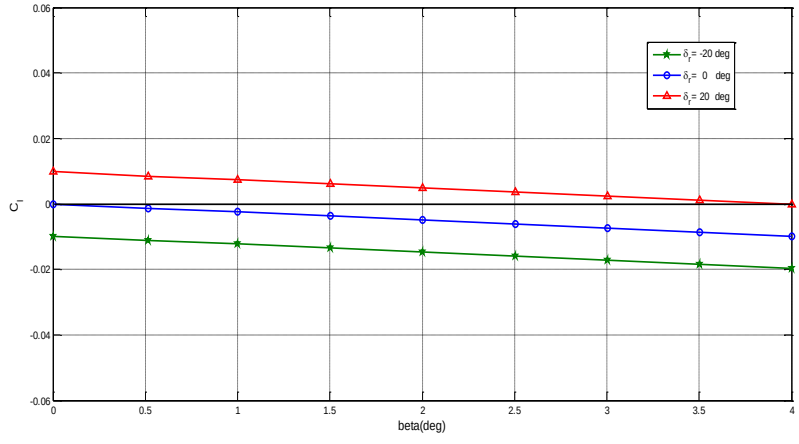

Figure 19: Variation of rolling moment coefficient curve with rudder deflection

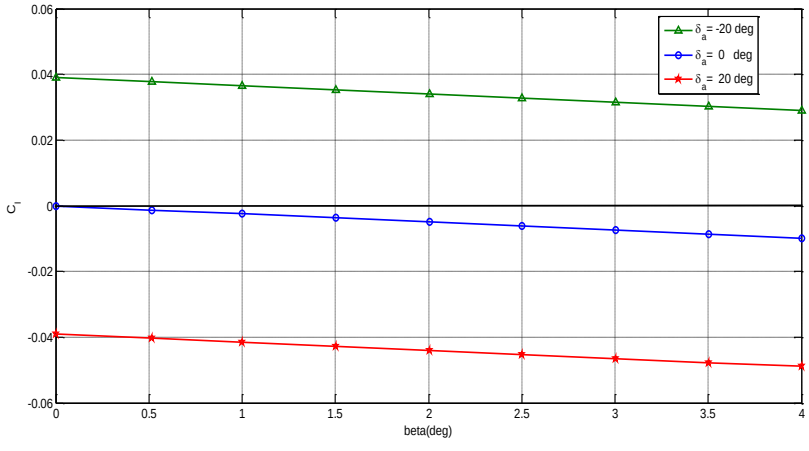

Figure 20: Variation of rolling moment coefficient curve with aileron deflection

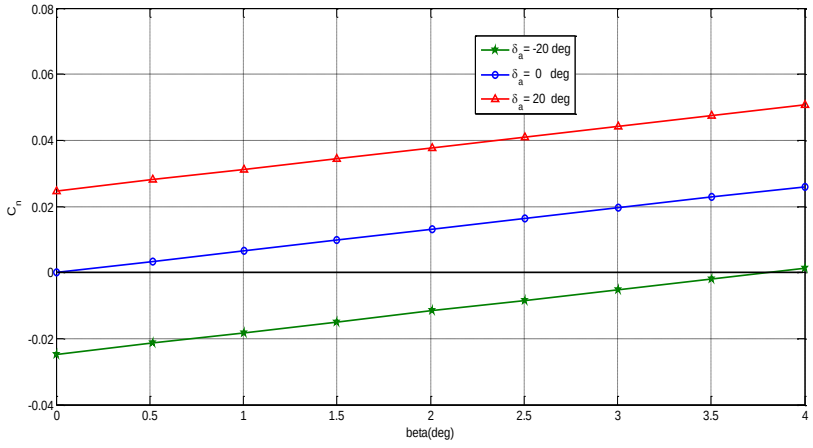

Figure 21: Variation of yawing moment coefficient curve with aileron deflection

7. CONCLUSION

This work presents the importance of using the panel method technique for the solution of the flow around 3D bodies. A good agreement was obtained between the numerical solutions when compared with experimental published data for three dimensional wings and DATCOM for the flow around Airbus A380 aircraft. The approach revealed to be faster in calculations than other numerical methods (finite difference, finite volume and finite element) since the solution is at the body surface only.

REFERENCES

[1] H. N. V. Dutt, B. Rajeswari, *Constant Source Panel Method for Analysis of Potential Flow Over Arbitrary Bodies*, National Aeronautical Laboratory, Bangalore, India, August 1986.

[2] D. A. Caughey, *Incompressible Potential Flow, Text Book*, Sibley School of Mechanical & Aerospace Engineering, October 3, 2008.

[3] M. Tarkian and F. J. Z. Tessier, *Aircraft Parametric 3D Modeling and Panel Code Analysis for Conceptual Design*, Linkoping University, February 8, 2007.

[4] C. Pozrikidis, *Fluid Dynamics, Theory, Computation, and Numerical Simulation*, Kluwer Academic Publisher, 2001.

[5] J. L. Hess and A. M. O Smith, *Calculation of Potential Flow about Arbitrary Bodies*, Douglas Aircraft Company, 1969.

[6] W. H. Mason, *Applied Computational Aerodynamics*, Text Book, January 23, 1997.

[7] J. Katz and A. Plotkin, *Low Speed Aerodynamics*, McGraw-Hill, Inc, New York, 1991.

[8] S. M. Richadson and A. R. H. Cornish, *Solution of Three Dimensional Incompressible Flow problem*, *J. Fluid Mech.* volume **82**, pp.309-319, 1977.